THE JOURNAL OF PHYSICAL CHEMISTRY C

Article

Cite This: J. Phys. Chem. C 2019, 123, 21564−21570

pubs.acs.org/JPCC

Rapid Laser-Induced Temperature Jump Decomposition of the Nerve Agent Simulant Diisopropyl Methylphosphonate under Atmospheric Conditions

Rebecca S. Thompson,[†] Michelle R. Brann,[†] Ellen H. Purdy, Jacob D. Graham, Alison A. McMillan, and S. J. Sibener*

The James Franck Institute and Department of Chemistry, The University of Chicago, 929 E. 57th Street, Chicago, Illinois 60637, United States

ABSTRACT: We present work detailing the destruction of the nerve agent simulant diisopropyl methylphosphonate (DIMP) via rapid laser heating under atmospheric conditions. Following Nd:YAG laser ablation of liquid DIMP deposited on a graphite substrate, both parent and product fragments are transmitted via capillary from an atmospheric chamber to a vacuum chamber containing a high-resolution mass spectrometer. This allows for real-time measurements of product distributions under a variety of temperature and atmospheric conditions. Ex situ Fourier transform infrared (FTIR) spectroscopy analysis of the same chamber contents provides complementary information about product identities and fragmentation pathways. Results demonstrate that product distributions depend on heating rate, surface temperature, and atmospheric oxygen content. In the destruction of the DIMP, the relative yields of alkene products depends significantly on laser power; smaller products are relatively more abundant at higher ablation temperatures. We also show that in the absence of atmospheric oxygen, the concentration of oxygenated products decreases sharply relative to alkene and alkane products. This suggests that under high-temperature conditions, atmospheric oxygen is incorporated directly into the products of the fragmented simulant. This project extends significantly our understanding of the fundamental chemistry of these dangerous compounds under atmospheric and rapidly changing thermal conditions. The results have critical implications for the development of effective chemical warfare agent decontamination and destruction strategies.

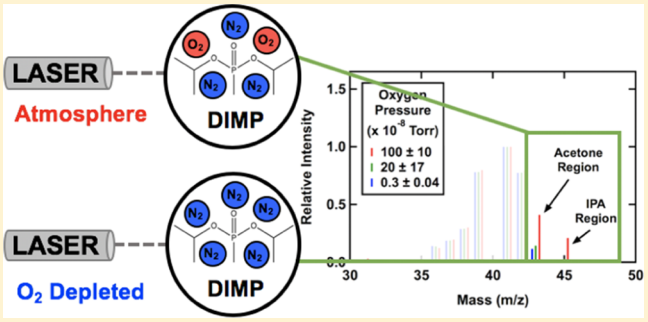

INTRODUCTION

Because of the threat chemical warfare agents (CWAs) pose to the global community, there is considerable interest in detecting, destroying existing stockpiles, and decontaminating areas affected by these compounds.[1,2] Current large-scale destruction techniques include incineration[3] and neutralization by base hydrolysis, but these strategies come with additional challenges regarding safe transport and toxic byproducts.[4] Therefore, it remains critical to continue developing new strategies and to understand the exact chemistry of agents' destruction in both vapor and condensed phases. Of particular interest are the extremely dangerous organophosphonate nerve agents Soman and Sarin.[5] Sarin, for example, has a high estimated toxicity of 35 mg min m^{-3} in humans via vapor inhalation.[6] Even beyond these dangerous compounds, many less toxic organophosphonates have found widespread industrial use as plasticizers, flame retardants, fire-resistant fluids and lubricants, and pesticides.[7,8] It is therefore important to characterize environmental impacts and remediation strategies for organophosphonate contaminants more broadly. This study adds to our fundamental understanding of the primary chemical kinetics and physical processes occurring when these compounds are exposed to rapid heating under atmospheric conditions.

The current work presents a detailed investigation of the laser-induced, high-temperature rapid heating destruction of the nerve agent simulant diisopropyl methylphosphonate (DIMP, Figure 1).[9−11] DIMP was selected from among the class of organophosphonate simulants for two reasons. First,

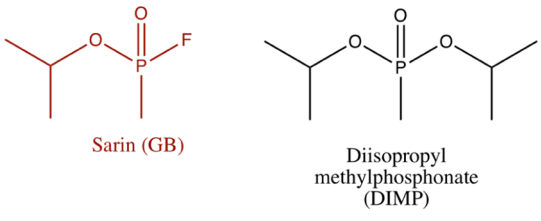

Figure 1. Chemical structures of the nerve agent Sarin (red) and the simulant DIMP (black) differ only in the replacement of fluorine with an additional oxygen and isopropyl group.

Received: June 5, 2019
Revised: July 24, 2019
Published: August 23, 2019

DOI: 10.1021/acs.jpcc.9b05381
J. Phys. Chem. C 2019, 123, 21564−21570

DIMP shares key structural similarities with the nerve agent Sarin, which is a compound of particular interest due in part to its use in urban terror attacks in Japan and its exposure to US troops abroad.[4,9] Second, it has been shown in a number of pyrolytic and thermal studies that a significant organophosphonate destruction channel yields substituted and unsubstituted carbon products resulting from the alkoxy moiety.[11−18] This gaseous product array is easily detectible and differentiable via mass spectrometry (MS) and Fourier transform infrared (FTIR) analyses, which enables a robust investigation of the impact of laser heating rate, surface temperature, and atmospheric pressure on simulant destruction.

In addition to experimental and theoretical work on the thermal decomposition and combustion of these compounds,[11,17,19−21] this work is an extension of previous studies examining oxidative[22,23] and laser destruction[24] of adsorbed chemical nerve agent simulants under ultrahigh vacuum conditions. The oxidative destruction of DIMP and dimethyl methylphosphonate (DMMP) progresses at similar rates and yields oxygen- and carbonyl-containing oligomeric product species.[22,23] Laser desorption and destruction studies of a number of Sarin simulants, (DIMP, DMMP, and diethyl ethylphosphonate), demonstrated lower temperature thresholds for destruction of simulants with relatively larger phosphonate side chains.[24] On the basis of these results, we again expect that the majority of gas-phase products in this study will include a variety of 1, 2, and 3-carbon products generated from the DIMP isopropyl group, with possible incorporation of atmospheric oxygen.

Using a unique atmospheric pressure ablation chamber, rapid laser heating of 10^{11} K s^{-1}, and in situ MS, this work probes the reaction products in the prompt destruction of DIMP under atmosphere and, for the first time, oxygen-depleted atmospheric conditions. In addition to identifying product branching ratios as a function of laser power, the manipulation of oxygen content allows us to elucidate the mechanistic role of oxygen in simulant destruction. This basic understanding is critical for practical decontamination strategies that involve, for example, flame incineration, as these conditions often lead to significant oxygen depletion in the local environment.[25]

In the laser-induced thermal destruction of DIMP, we demonstrate that the resulting product distribution is dependent on both surface temperature rise and atmospheric oxygen composition. More specifically, the relative production of small alkene products depends significantly on laser power; the relative yield of smaller substituted products is higher when the sample is ablated with higher laser powers. Likewise, under oxygen-depleted conditions, the relative amount of oxygenated products decreases sharply relative to alkene and alkane products. This suggests that under extreme high-temperature conditions, atmospheric oxygen is incorporated directly into the products of the fragmented simulant. Such findings are directly relevant to producing novel CWA mitigation strategies and maintaining national security.

EXPERIMENTAL SECTION

All experiments were conducted in a newly constructed atmospheric-MS apparatus, shown in Figure 2. Additional measurements were collected via ex situ FTIR analysis. In short, a UTI 100 quadrupole mass spectrometer (QMS) occupies a high-vacuum chamber reaching base pressures of

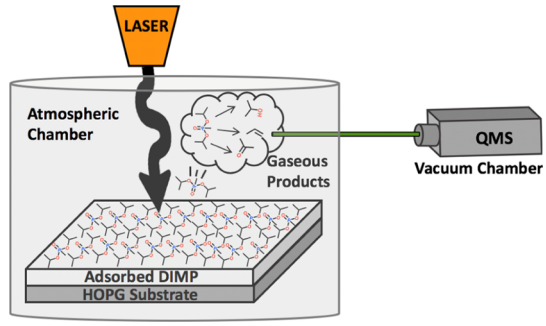

Figure 2. Laser ablation experiments are conducted in a joint atmospheric and high-vacuum apparatus. A Nd:YAG laser is used to ablate DIMP simulant films in an atmospheric chamber (purple). Gaseous products are transported via capillary (green) to a high-vacuum chamber containing a UTI QMS for analysis.

10^{-9} Torr. This chamber samples, via a 20 cm fused silica capillary with a 25 μm inner diameter, the gaseous products produced in a small, adjacent atmospheric chamber used for laser ablation trials. A second identical inlet capillary in the atmospheric chamber ensures that atmospheric pressure is maintained during experimental sampling. The volume of the atmospheric sampling chamber is small (approximately 40 cm^3), which enables rapid diffusion of vapor products; changes in chamber contents are detected by the mass spectrometer within 300 ms. We do note that the capillary is not heated, so there is a possibility for vapor condensation of DIMP or associated products during transport. Gas-phase products are, however, expected to thermalize rapidly in the atmospheric chamber, so we do not expect condensation in the capillary to be a major pathway. The large pressure differential between the two chambers also ensured consistent gas flow through the capillary and repeated use of the same capillary showed no blockage, indicating that condensation was not happening on a large scale.

In order to prepare DIMP samples for ablation, the atmospheric chamber was routinely purged and re-opened to atmosphere between trials. The substrate for all experiments was a highly ordered pyrolytic graphite crystal [highly oriented pyrolytic graphite (HOPG), Bruker]. In addition to chamber purging, the HOPG surface was exfoliated between trials to ensure reproducible surface quality and composition. To begin each experiment, 10 μL of DIMP (Alfa Aesar) was deposited on the HOPG surface, and the chamber was sealed. A background mass scan was then collected; final product analysis was performed on the background-subtracted spectra collected following ablation.

DIMP films were ablated with a Nd:YAG laser (Quanta-Ray GCR 130) producing near-IR photons at 1064 nm. To estimate the surface temperature on the HOPG substrate induced by the laser pulse, the following calculation was carried out for one-dimensional heat flow into a semi-infinite slab of material (transverse propagation of the beam is large compared to the depth of heat conduction into the film). Assuming that the optical absorption coefficient of HOPG is large (on the order of 10^4−10^6 cm^{-1}),[26−29] the surface temperature of the HOPG surface at time t can be calculated as[30]

$$T(0, t) = \frac{2F_0}{K}\left(\frac{\kappa t}{\pi}\right)^{1/2} \quad (1)$$

DOI: 10.1021/acs.jpcc.9b05381
J. Phys. Chem. C 2019, 123, 21564−21570

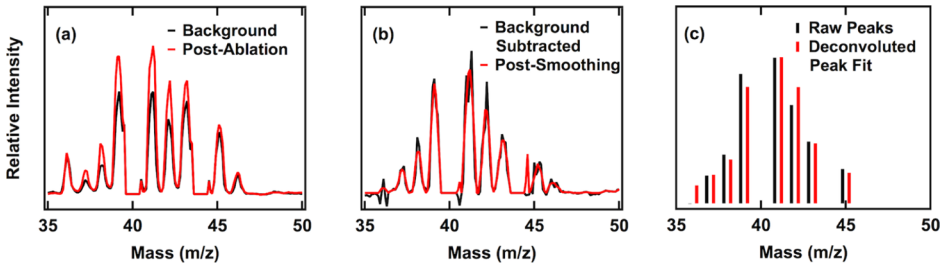

Figure 3. Representative mass spectra for ablated DIMP are processed and analyzed. Background spectra are subtracted from postablation spectra (a). These background-subtracted spectra are smoothed (red, b) and peaks are detected (black bars, c). A least-squares procedure is used to determine relative product yields and reproduce the ablated spectra (red bars, c).

In eq 1, F_0 is the absorbed incident flux from the laser, K is the thermal conductivity of HOPG, and κ is the thermal diffusivity (reported as 290 W m^{-1} K^{-1} and 0.000165 m^2 s, respectively).[31] In practice, the total pulsed laser power is first measured with a Scientech calorimeter (model 38-0101). This output is then converted to pulse energy by incorporating the pulse frequency (20 Hz) and scaling to the duration of individual pulses (8 ns). Pulse energies in this study range from 0.103 to 0.244 J. This total flux is further scaled to the reflection coefficient of HOPG (reported as 0.21 at 300 K).[26] With this model, peak laser powers raise the crystal temperature to approximately 2830 ± 110 K at a heating rate of 3.2×10^{11} K s^{-1}. The error cited for temperature is a standard propagation including error from the calorimeter measurement, pulse width, and HOPG reflection coefficient. We note that simulant films were ablated for 2 min at 20 Hz in order to generate sufficient product signal for analysis. However, product signals (propene at m/z = 41, e.g.) were detected for single pulse ablations, and thermocouple measurements of the HOPG crystal show a steady-state temperature rise of only approximately 350 K as a result of the extended ablation. Therefore, we assume that the modest temperature rise caused by extended ablation is negligible compared to the high temperatures during each individual pulse.

Mass spectra analyses involved a series of steps illustrated with representative data in Figure 3. To begin, background spectra were subtracted from postablation spectra (Figure 3a). Next, the MALDIquant R package was used for data smoothing (using a 7-point Savitzky−Golay-filter, Figure 3b) and peak detection.[32,33] In order to deconvolve the spectra into individual product contributions, it was first necessary to build a library of fragmentation patterns for the proposed products. To this end, mass spectra were collected for propene (Sigma-Aldrich), acetone, and isopropyl alcohol (IPA, both from Fisher Scientific). The spectra for additional products, ethylene and acetylene, were obtained from reference data from the National Institute of Standards and Technology.[34] Once this library was complete, the relative product contributions for the ablated spectra were determined using a least-squares analysis (Figure 3c). We note that though present in the background-subtracted spectra, large peaks associated with atmospheric gases like N_2, O_2, Ar, and so forth, were excluded from this deconvolution procedure because of the difficulty separating trace product signals from atmospheric contributions. The omission of m/z = 27 and 28 in particular made it difficult to distinguish ethylene and acetylene. Therefore, all discussions herein will group these two-carbon products together.

In addition to MS, a second modular chamber was used for concurrent ex situ FTIR analysis of ablated products. To begin these experiments, a 150 cm^3 IR cell with ZnSe windows was purged to approximately 25 mTorr. This chamber was connected via a leak valve to an analogous atmospheric chamber for simulant ablation. Following the ablation procedure, the valve was opened, allowing the evolved gaseous products to escape into the purged chamber. The contents of the unheated chamber were analyzed using a Nicolet iS50 infrared spectrophotometer (Thermo Fisher) and a liquid nitrogen-cooled MCT/A detector. All such FTIR spectra were averaged over 200 scans at 4 cm^{-1} resolution; peak fitting analysis utilized Gaussian peaks atop cubic baselines.

RESULTS AND DISCUSSION

FTIR Product Analysis. Previous investigations into the thermal destruction of DIMP have consistently identified a number of products including propene, IPA, and ethylene. These studies include destruction via pyrolysis, combustion, exposure to a corona discharge, dissociative adsorption, laser ablation, and so forth.[1,11,12,35−37] While this provides a reasonable set of products to look for, the current work represents the first direct study of rapid laser heating (on the order of 10^{11} K s^{-1}) of adsorbed liquid DIMP under atmospheric pressure and oxygen-depleted conditions. It is therefore necessary to firmly establish the full range of products before attempting to assess branching ratios; this was done using ex situ FTIR. Representative spectra of ablated DIMP in Figure 4 show clear evidence of propene, ethylene,

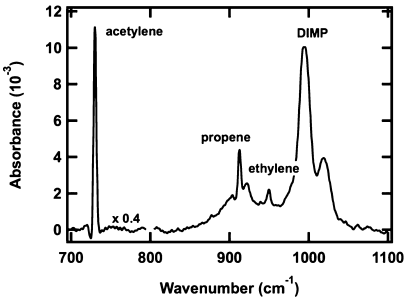

Figure 4. Representative FTIR spectra of DIMP ablated to approximately 2720 K shows clear evidence of residual DIMP as well as acetylene, propene, and ethylene products.

acetylene, as well as contributions from unreacted DIMP or other partially decomposed organophosphonate fragments such as isopropyl methylphosphonate (IMP). In addition to the prominent phosphonate P−O−C stretching modes at 995 and 1020 cm^{-1}, we observe significant signal intensity from propene's $=CH_2$ wagging mode (912 cm^{-1}) and the bending modes of acetylene and ethylene (730 cm^{-1} and 949 cm^{-1},

DOI: 10.1021/acs.jpcc.9b05381
J. Phys. Chem. C 2019, 123, 21564−21570

respectively). All peaks referenced herein are consistent with those reported for the corresponding molecules in the gas phase.[10,38−44] CO is also observed, but this is difficult to uniquely assign to either DIMP or HOPG ablation. Additionally, other small product peaks are observed in the spectra beyond those highlighted in Figure 4, but we were not able to clearly establish their identities using FTIR alone.

In both FTIR and the following MS analyses, we note that the scope of our experiment did not include direct quantification of condensed-phase products or parent molecules remaining on the HOPG substrate or in the atmospheric chamber. Similar to other studies, however, our gas-phase product analysis suggests that it is primarily phosphorus-containing products that remain following thermal destruction.[11,45] In addition to unreacted DIMP, these products likely include IMP and methylphosphonic acid.

As laser power (and thereby HOPG surface temperature) is increased, an interesting trend emerges in the relative distribution of products. When spectra are normalized to the height of the propene peak, there is a corresponding relative increase in the height of ethylene (Figure 5a). If the relative

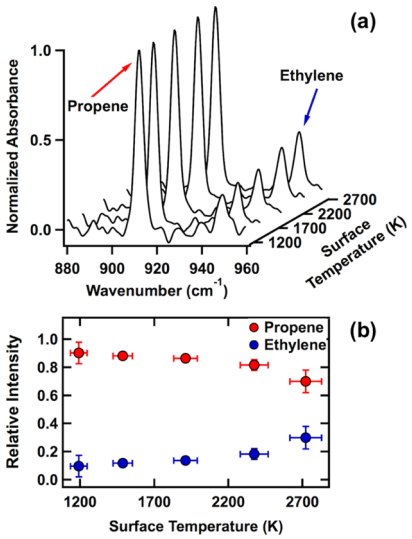

Figure 5. Relative production of ethylene and propene changes as a function of laser ablation power. FTIR spectra normalized to propene height (a) demonstrate increases in relative ethylene production as surface ablation temperature increases. Baseline and other product peaks have been subtracted for clarity. The relative integrated area of the associated peaks (b) shows that this trend is observed throughout the temperature range explored in this study (error bars represent the standard deviation of at least three trials at each ablation temperature).

areas of these two peaks are plotted as a function of HOPG surface temperature (Figure 5b), it becomes clear that as the ablation temperature increases, ethylene production increases relative to propene. The same trend is observed for relative propene and acetylene production. Without precise absorption cross-sections for these compounds, it is difficult to quantify the absolute amount of each product formed. It is clear, however, that higher temperatures lead to a higher yield of smaller substituted carbon products.

Effects of Varying Surface Temperature. The results described in the preceding section were easily replicated with in situ MS. However, it is important to note that the mass spectra data reveal some additional minor products unidentified in the FTIR data. FTIR spectra provided no conclusive evidence of oxygenated ablation products, despite their suggested presence in other pyrolytic and thermal decomposition studies of DIMP.[12,35,36] Background-subtracted mass spectra of ablated DIMP, however, show clear increases in m/z = 43 and m/z = 45 (acetone and IPA, respectively). The yield of both of these products is consistently small relative to propene and ethylene/acetylene, so their absence in FTIR spectra may simply be due to lack of sensitivity. Therefore, mass spectra are deconvoluted into contributions from four observed products: propene, ethylene/acetylene, acetone, and IPA. Figure 6 shows the least-squares fit for the data collected in three representative trials at different ablation powers. When the data are normalized to the propene signal (m/z = 41), there is a clear corresponding relative increase in the amount of the smaller acetylene and ethylene products. In other words, these results again suggest that peak surface temperatures impact the extent of bond cleavage and identity of destruction products.

Effects of Varying Atmospheric Oxygen. In order to probe the role of atmospheric oxygen in DIMP destruction, we performed a series of experiments with variable partial pressures of oxygen. Following simulant deposition, the sampling chamber was carefully purged with N_2 until a desired oxygen pressure was reached (as measured with the QMS). The chamber, however, was still maintained at atmospheric pressure. After ablation at the highest laser powers, the results in Figure 7 show that the presence of oxygenated products plummets nearly to zero when atmospheric oxygen is reduced. Signals associated with both acetone (m/z = 43) and IPA (m/z = 45) decrease sharply relative to propene (m/z = 41). This observation is of critical importance; it demonstrates clearly that atmospheric oxygen is incorporated directly into the fragmenting DIMP molecule.

Mechanism of Destruction. The effects of varying both ablation surface temperature and atmospheric composition are summarized in Table 1. Each entry represents the average of at least three similar trials. In brief, we observe that higher ablation temperatures lead to an increase in the relative production of shorter chain-substituted products (ethylene/acetylene vs propene). Additionally, a reduction in available atmospheric oxygen leads to a decrease in the relative production of oxygenated products (acetone and IPA vs propene). These results inform the following discussion of the mechanisms underlying the thermal destruction of condensed-phase DIMP.

To begin, it has been proposed experimentally and theoretically that the primary pyrolytic destruction step for DIMP and other similar molecules is a unimolecular decomposition to IMP and propene via a six-membered ring transition state.[11,46−48] Moreover, propene production has been observed under a variety of high-temperature conditions, beginning with temperatures as low as 700 K, which is lower than the ablation range studied here.[11,24] In vacuum studies, propene is also produced as a result of dissociative adsorption of DIMP.[13,37] Essentially, many studies agree that a major step in DIMP destruction involves the formation of propene. On the other hand, few studies have identified direct mechanisms that yield smaller substituted products from DIMP's initial dissociation (and indeed no single initial bond scission is enough to yield a two-carbon product from DIMP directly). Instead, it is likely that the smaller products (ethylene, acetylene, methane, etc) are produced as secondary

DOI: 10.1021/acs.jpcc.9b05381
J. Phys. Chem. C 2019, 123, 21564−21570

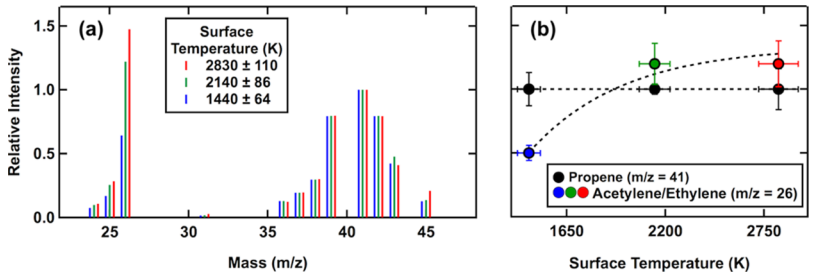

Figure 6. Reproduced representative mass spectra (a) from a least-squares fit of the data (normalized to propene signal at m/z = 41) show an increase in low molecular weight products (ethylene and acetylene) as laser power is increased. This can also be seen in the normalized relative intensities of propene and acetylene/ethylene (m/z = 26) averaged across all trials (b). Ablation surface temperatures are 1440 K (blue), 2140 K (green), and 2830 K (red). Dotted line is drawn to guide the eye.

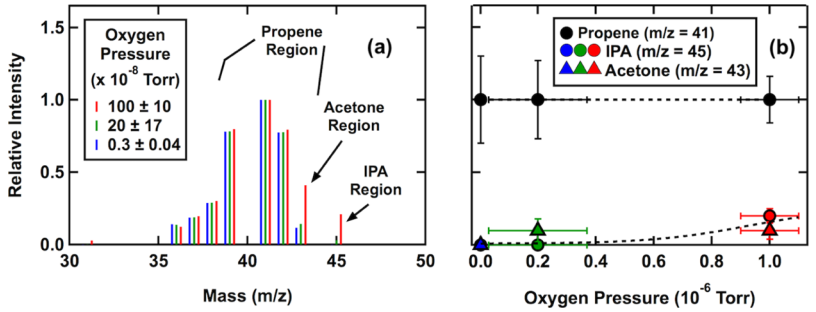

Figure 7. Reproduced representative mass spectra (a) from a least-squares fit of the data (normalized to propene signal at m/z = 41) show a sharp decrease in oxygenated products as available oxygen decreases. This can also be seen in the normalized relative intensities of propene, IPA (m/z = 45), and acetone (m/z = 43) averaged across all trials (b). Recorded oxygen pressures in the QMS chamber were 1×10^{-6} Torr under atmospheric ablation conditions (red), 2×10^{-7} under low oxygen conditions (green), and 3×10^{-9} Torr under oxygen-depleted conditions (blue). Dotted line is drawn to guide the eye.

Table 1. Summary of All DIMP Ablation Experiments Performed, Normalized to Propene Production[a]

Chamber Conditions		Relative Product Contributions			
Oxygen (Torr)	*Surface Temp (K)*	*IPA*	*Acetone*	*Propene*	*Ethylene/Acetylene*
$(1 \pm 0.1) \times 10^{-6}$	2830 ± 110	0.2 ± 0.05	0.1 ± 0.06	1 ± 0.16	1.2 ± 0.18
$(1 \pm 0.1) \times 10^{-6}$	2140 ± 86	0.2 ± 0.03	0.1 ± 0.12	1 ± 0.04	1.2 ± 0.16
$(1 \pm 0.1) \times 10^{-6}$	1440 ± 64	0.1 ± 0.08	0.4 ± 0.13	1 ± 0.13	0.5 ± 0.06
$(1 \pm 0.1) \times 10^{-6}$	2830 ± 110	0.2 ± 0.05	0.1 ± 0.06	1 ± 0.16	1.2 ± 0.18
$(2 \pm 1.7) \times 10^{-7}$	2830 ± 110	0 ± 0.03	0.1 ± 0.08	1 ± 0.27	4.2 ± 0.86
$(3 \pm 0.4) \times 10^{-9}$	2830 ± 110	0 ± 0.0	0 ± 0.0	1 ± 0.3	7 ± 1.49

[a]As surface temperature is increased, the relative ratio of ethylene and acetylene to propene increases (red). As available oxygen is decreased, the relative production of IPA and acetone decreases (blue).

destruction products of propene.[49,50] The results of this work present evidence that indeed propene is likely one of the first products, and that higher ablation temperatures increase the relative extent of further fragmentation.

The results of the oxygen study add interesting detail to the existing mechanistic picture. Zegers and Fisher proposed a two-step pyrolysis mechanism for DIMP, beginning with the unimolecular decomposition that yields propene. The second step involves transfer of a hydrogen from the phosphorous hydroxyl group to the oxygen of the isopropoxy group, yielding IPA and methyl dioxophosphorane.[11,51] Our observations suggest, however, that this intermolecular step may not be the primary mechanism for IPA formation at these high-temperature, fast-heating, and condensed-phase conditions. Instead, atmospheric O_2 or radicals formed from thermal dissociation may abstract hydrogens or break bonds in the DIMP molecule directly. For example, if an alkyl radical forms upon scission of the P−O−C bond, atmospheric O_2 can readily add to generate an alkoxy radical. This species, in turn, is expected to react or decompose readily to form both the observed acetone and IPA.[52−54] The direct incorporation of oxygen from the atmosphere in this proposed mechanism would account for the observed dependence on oxygen pressure in the ablation chamber in the production of oxygenated products.

CONCLUSIONS

Building on work investigating pyrolysis, dissociative adsorption, and laser ablation of CWAs and their simulants, this study presents a comprehensive look at rapid thermal ablation of condensed DIMP, a simulant of Sarin, under atmospheric pressure conditions. Decomposition products observed include propene, ethylene, acetylene, IPA, and acetone, which are well in line with existing literature on thermal destruction of organophosphonates. Product distributions varied significantly when both laser power (HOPG surface temperature) and oxygen content were altered; higher ablation powers led to higher temperatures, which increased the extent of secondary fragmentation in alkene and alkyne products observed. Lower

DOI: 10.1021/acs.jpcc.9b05381
J. Phys. Chem. C 2019, 123, 21564−21570

oxygen partial pressures led to a sharp decrease in oxygenated products, suggesting that a dominating mechanism in this system involves direct incorporation of atmospheric oxygen into product fragments.

Though Sarin, unlike DIMP, includes a fluorine substituent on the central phosphorus atom, there is reason to believe that the results highlighted here have direct relevance for Sarin's thermal destruction. Experimental work with simulants and nerve agents has shown significant correlation between bond frequency and desorption energies, suggesting that simulants like DIMP are indeed appropriate for modeling the chemistry of toxic agents.[9] Perhaps more importantly, pyrolytic simulations of Sarin have confirmed that thermal destruction begins with the same six-center intermediate that leads to propene elimination.[21] Therefore, we expect that the chemistry observed in these temperature-jump experiments is relatively generalizable to Sarin and other large organophosphonates.

In addition to validating the applicability of these results on live nerve agents, extensions of this work may include tracking the destruction temperature thresholds and product distributions for additional simulants and simulant mixtures, as well as the impact of incorporating less absorptive or reactive substrates. In general, this work continues to shed light on the basic mechanisms of organophosphonate thermal destruction, related to those encountered under high-temperature rapid-heating blast conditions. These results are critical for the accurate modeling of environmental persistence and implementation of mitigation strategies for CWAs and other organophosphonate pesticides.

AUTHOR INFORMATION

Corresponding Author

*E-mail: s-sibener@uchicago.edu.

ORCID

S. J. Sibener: 0000-0002-5298-5484

Author Contributions

†R.S.T. and M.R.B. contributed equally to this work and are co-first authors of this manuscript.

Notes

The authors declare no competing financial interest.

ACKNOWLEDGMENTS

This work was sponsored by the Defense Threat Reduction Agency (DTRA) under grant no. HDTRA1-16-1-0024. Additional support was provided by the NSF Materials Research Science and Engineering Center at The University of Chicago, grant no. NSF-DMR-14-20709 as well as by the Core Spectrometry Facility at the University of Chicago, grant no. NSF-CHE-1048528.

REFERENCES

(1) Korobeinichev, O. P.; Chernov, A. A.; Sokolov, V. V.; Krasnoperov, L. N. Kinetics of Destruction of Diisopropyl Methylphosphonate in Corona Discharge. *Int. J. Chem. Kinet.* **2002**, *34*, 331−337.

(2) Korobeinichev, O. P.; Ilyin, S. B.; Shvartsberg, V. M.; Chernov, A. A. The Destruction Chemistry of Organophosphorus Compounds in Flames—I: Quantitative Determination of Final Phosphorus-Containing Species in Hydrogen-Oxygen Flames. *Combust. Flame* **1999**, *118*, 718−726.

(3) Ganesan, K.; Raza, S. K.; Vijayaraghavan, R. Chemical Warfare Agents. *J. Pharm. BioAllied Sci.* **2010**, *2*, 166−178.

(4) Kim, K.; Tsay, O. G.; Atwood, D. A.; Churchill, D. G. Destruction and Detection of Chemical Warfare Agents. *Chem. Rev.* **2011**, *111*, 5345−5403.

(5) Munro, N. B.; Talmage, S. S.; Griffin, G. D.; Waters, L. C.; Watson, A. P.; King, J. F.; Hauschild, V. The Sources, Fate, and Toxicity of Chemical Warfare Agent Degradation Products. *Environ. Health Perspect.* **1999**, *107*, 933−974.

(6) National Research Council. Review of Acute Human-Toxicity Estimates for GB (Sarin). *Review of Acute Human-Toxicity Estimates for Selected Chemical-Warfare Agents*; National Academies Press (US): Washington (DC), 1997; pp 28−34.

(7) Szinicz, L. History of Chemical and Biological Warfare Agents. *Toxicology* **2005**, *214*, 167−181.

(8) Aschmann, S. M.; Tuazon, E. C.; Atkinson, R. Atmospheric Chemistry of Diethyl Methylphosphonate, Diethyl Ethylphosphonate, and Triethyl Phosphate. *J. Phys. Chem. A* **2005**, *109*, 2282−2291.

(9) Davis, E. D.; Gordon, W. O.; Wilmsmeyer, A. R.; Troya, D.; Morris, J. R. Chemical Warfare Agent Surface Adsorption: Hydrogen Bonding of Sarin and Soman to Amorphous Silica. *J. Phys. Chem. Lett.* **2014**, *5*, 1393−1399.

(10) Wilmsmeyer, A. R.; Gordon, W. O.; Davis, E. D.; Troya, D.; Mantooth, B. A.; Lalain, T. A.; Morris, J. R. Infrared Spectra and Binding Energies of Chemical Warfare Nerve Agent Simulants on the Surface of Amorphous Silica. *J. Phys. Chem. C* **2013**, *117*, 15685−15697.

(11) Zegers, E. J. P.; Fisher, E. M. Gas-Phase Pyrolysis of Diisopropyl Methylphosphonate. *Combust. Flame* **1998**, *115*, 230−240.

(12) Glaude, P. A.; Melius, C.; Pitz, W. J.; Westbrook, C. K. Detailed Chemical Kinetic Reaction Mechanisms for Incineration of Organophosphorus and Fluoroorganophosphorus Compounds. *Proc. Combust. Inst.* **2002**, *29*, 2469−2476.

(13) Kuiper, A.; Vanbokhoven, J.; Medema, J. The Role of Heterogeneity in the Kinetics of a Surface Reaction. I. Infrared Characterization of the Adsorption Structures of Organophosphonates and Their Decomposition. *J. Catal.* **1976**, *43*, 154−167.

(14) Zegers, E. J. P.; Fisher, E. M. Gas-Phase Pyrolysis of Diethyl Methylphosphonate. *Combust. Sci. Technol.* **1996**, *116-117*, 69−89.

(15) Paciorek, K. J. L.; Kratzer, R. H.; Kaufman, J.; Nakahara, J. H.; Christos, T.; Hartstein, A. M. Thermal Oxidative Degradation Studies of Phosphate Esters. *Am. Ind. Hyg. Assoc. J.* **1978**, *39*, 633−639.

(16) Lhomme, V.; Bruneau, C.; Soyer, N.; Brault, A. Thermal Behavior of Some Organic Phosphates. *Ind. Eng. Chem. Prod. Res. Dev.* **1984**, *23*, 98−102.

(17) Higgins, C. E.; Baldwin, W. H. The Thermal Decomposition of Tributyl Phosphate 1. *J. Org. Chem.* **1961**, *26*, 846−850.

(18) Bruneau, C.; Soyer, N.; Brault, A.; Kerfanto, M. Thermal Degradation of Tri-n-Butyl Phosphate. *J. Anal. Appl. Pyrolysis* **1981**, *3*, 71−81.

(19) Yang, L.; Shroll, R. M.; Zhang, J.; Lourderaj, U.; Hase, W. L. Theoretical Investigation of Mechanisms for the Gas-Phase Unimolecular Decomposition of DMMP. *J. Phys. Chem. A* **2009**, *113*, 13762−13771.

(20) Glaude, P. A.; Curran, H. J.; Pitz, W. J.; Westbrook, C. K. Kinetic Study of the Combustion of Organophosphorus Compounds. *Proc. Combust. Inst.* **2000**, *28*, 1749−1756.

(21) Glaude, P. A.; Melius, C.; Pitz, W. J.; Westbrook, C. K. Detailed Chemical Kinetic Reaction Mechanisms for Incineration of Organophosphorus and Fluoroorganophosphorus Compounds. *Proc. Combust. Inst.* **2002**, *29*, 2469−2476.

(22) Thompson, R. S.; Langlois, G. G.; Sibener, S. J. Oxidative Destruction of Multilayer Diisopropyl Methylphosphonate Films by $O(^3P)$ Atomic Oxygen. *J. Phys. Chem. B* **2018**, *122*, 455−463.

(23) Langlois, G. G.; Thompson, R. S.; Li, W.; Sibener, S. J. Oxidation, Destruction, and Persistence of Multilayer Dimethyl Methylphosphonate Films during Exposure to $O(^3P)$ Atomic Oxygen. *J. Phys. Chem. C* **2016**, *120*, 16863−16870.

DOI: 10.1021/acs.jpcc.9b05381
J. Phys. Chem. C 2019, 123, 21564−21570

(24) Gibson, K. D.; Sibener, S. J. Fate of Some Chemical Warfare Simulants Adsorbed on an Inert Surface When Exposed to Rapid Laser Initiated Heating. *J. Phys. Chem. C* **2018**, *122*, 24684−24689.
(25) Oppelt, E. T. Incineration Of Hazardous Waste. *JAPCA* **1987**, *37*, 558−586.
(26) Bulgakova, N. M.; Bulgakov, A. V. Pulsed Laser Ablation of Solids: Transition from Normal Vaporization to Phase Explosion. *Appl. Phys. A: Mater. Sci. Process.* **2001**, *73*, 199−208.
(27) Smausz, T.; Kondász, B.; Gera, T.; Ajtai, T.; Utry, N.; Pintér, M.; Kiss-Albert, G.; Budai, J.; Bozóki, Z.; Szabó, G.; et al. Determination of UV−Visible−NIR Absorption Coefficient of Graphite Bulk Using Direct and Indirect Methods. *Appl. Phys. A: Mater. Sci. Process.* **2017**, *123*, 633.
(28) Schultrich, B. Carbon Ablation with ns Lasers. *Tetrahedrally Bonded Amorphous Carbon Films*; Springer: Berlin, Heidelberg, 2018; pp 585−631.
(29) Kononenko, V. V.; Kononenko, T. V.; Pimenov, S. M.; Sinyavskii, M. N.; Konov, V. I.; Dausinger, F. Effect of the Pulse Duration on Graphitisation of Diamond during Laser Ablation. *Quantum Electron.* **2005**, *35*, 252−256.
(30) Ready, J. F. *Effects of High-Power Laser Radiation*; Academic Press: New York, NY, 1971.
(31) Windholz, R.; Molian, P. A. Nanosecond Pulsed Excimer Laser Machining of Chemically Vapour-Deposited Diamond and Graphite: Part II Analysis and Modelling. *J. Mater. Sci.* **1998**, *33*, 523−528.
(32) Gibb, S.; Strimmer, K. MALDIquant: A Versatile R Package for the Analysis of Mass Spectrometry Data. *Bioinformatics* **2012**, *28*, 2270−2271.
(33) Savitzky, A.; Golay, M. J. E. Smoothing and Differentiation of Data by Simplified Least Squares Procedures. *Anal. Chem.* **1964**, *36*, 1627−1639.
(34) Stein, S. E. Mass Spectra. In *NIST Chemistry WebBook*; Linstrom, P. J., Mallard, W. G., Eds.; NIST Standard Reference Database Number 69; National Institute of Standards and Technology: Gaithersburg MD, July 18, 2018.
(35) Korobeinichev, O. P.; Shvartsberg, V. M.; Shmakov, A. G. The Chemistry of Combustion of Organophosphorus Compounds. *Russ. Chem. Rev.* **2007**, *76*, 1094−1121.
(36) Radziemski, L. J. Laser-induced Photodestruction of the Organo-phosphates: DIMP and DMMP. *J. Environ. Sci. Health, Part B* **1981**, *16*, 337−361.
(37) Templeton, M. K.; Weinberg, W. H. Decomposition of Phosphonate Esters Adsorbed on Aluminum Oxide. *J. Am. Chem. Soc.* **1985**, *107*, 774−779.
(38) Guilbault, G. G.; Scheide, E.; Das, J. An Experimental Technique for Studying the Infrared Spectrum of Chemisorbed Compounds. *Spectrosc. Lett.* **1968**, *1*, 167−175.
(39) Crooks, R. M.; Yang, H. C.; McEllistrem, L. J.; Thomas, R. C.; Ricco, A. J. Interactions between Self-Assembled Monolayers and an Organophosphonate Detailed Study Using Surface Acoustic Wave-Based Mass Analysis, Polarization Modulation-FTIR Spectroscopy and Ellipsometry. *Faraday Discuss.* **1997**, *107*, 285−305.
(40) van Hest, M. F. A. M.; de Graaf, A.; van de Sanden, M. C. M.; van Hest, M. F. A. M.; Schram, D. C. Use of in Situ FTIR Spectroscopy and Mass Spectrometry in an Expanding Hydrocarbon Plasma. *Plasma Sources Sci. Technol.* **2000**, *9*, 615−624.
(41) Kaiser, R. I.; Roessler, K. Theoretical and Laboratory Studies on the Interaction of Cosmic-Ray Particles with Interstellar Ices. III. Suprathermal Chemistry−Induced Formation of Hydrocarbon Molecules in Solid Methane (CH_4), Ethylene (C_2H_4), and Acet. *Astrophys. J.* **1998**, *503*, 959−975.
(42) Silvi, B.; Labarbe, P.; Perchard, J. P. Spectres de Vibration et Coordonnées Normales de Quatre Espèces Isotopiques de Propène. *Spectrochim. Acta, Part A* **1973**, *29*, 263−276.
(43) Es-sebbar, E.-t.; Alrefae, M.; Farooq, A. Infrared Cross-Sections and Integrated Band Intensities of Propylene: Temperature-Dependent Studies. *J. Quant. Spectrosc. Radiat. Transfer* **2014**, *133*, 559−569.
(44) Stein, S. E. Infrared Spectra. In *NIST Chemistry WebBook*; Linstrom, P. J., Mallard, W. G., Eds.; NIST Standard Reference Database Number 69; National Institute of Standards and Technology: Gaithersburg MD, July 18, 2018.
(45) Yuan, B.; Eilers, H. T-Jump Pyrolysis and Combustion of Diisopropyl Methylphosphonate. *Combust. Flame* **2019**, *199*, 69−84.
(46) Shan, X.; Vincent, J. C.; Kirkpatrick, S.; Walker, M. D.; Sambrook, M. R.; Clary, D. C. A Combined Theoretical and Experimental Study of Sarin (GB) Decomposition at High Temperatures. *J. Phys. Chem. A* **2017**, *121*, 6200−6210.
(47) Ash, T.; Debnath, T.; Banu, T.; Das, A. K. Exploration of Unimolecular Gas-Phase Detoxication Pathways of Sarin and Soman: A Computational Study from the Perspective of Reaction Energetics and Kinetics. *Chem. Res. Toxicol.* **2016**, *29*, 1439−1457.
(48) Hahn, D. K.; RaghuVeer, K. S.; Ortiz, J. V. Computational Tests of Models for Kinetic Parameters of Unimolecular Reactions of Organophosphorus and Organosulfur Compounds. *J. Phys. Chem. A* **2011**, *115*, 14143−14152.
(49) Hidaka, Y.; Nakamura, T.; Tanaka, H.; Jinno, A.; Kawano, H.; Higashihara, T. Shock Tube and Modeling Study of Propene Pyrolysis. *Int. J. Chem. Kinet.* **1992**, *24*, 761−780.
(50) Davis, S. G.; Law, C. K.; Wang, H. Propene Pyrolysis and Oxidation Kinetics in a Flow Reactor and Laminar Flames. *Combust. Flame* **1999**, *119*, 375−399.
(51) Glaude, P. A.; Melius, C.; Pitz, W. J.; Westbrook, C. K. Detailed Chemical Kinetic Reaction Mechanisms for Incineration of Organophosphorus and Fluoroorganophosphorus Compounds. *Proc. Combust. Inst.* **2002**, *29*, 2469−2476.
(52) Milne, G. S.; Steel, C. The Gas-Phase Oxidation of Photochemically Generated Isopropyl Radicals. *J. Phys. Chem.* **1968**, *72*, 3754−3761.
(53) Atkinson, R.; Carter, W. P. L. Reactions of Alkoxy Radicals under Atmospheric Conditions: The Relative Importance of Decomposition versus Reaction with O_2. *J. Atmos. Chem.* **1991**, *13*, 195−210.
(54) Wijnen, M. J. H. Reactions of Alkoxy Radicals. VI. Photolysis of Isopropyl Propionate. *J. Am. Chem. Soc.* **1960**, *82*, 1847−1849.

DOI: 10.1021/acs.jpcc.9b05381
J. Phys. Chem. C 2019, 123, 21564−21570